

<https://doi.org/10.1038/s42003-024-06765-7>

# Stress responses in an Arctic microalga (Pelagophyceae) following sudden salinity change revealed by gene expression analysis

Check for updates

Nastasia J. Freyria<sup>1,2,3</sup>✉, Thais C. de Oliveira<sup>1,2,4</sup>, Mansi Chovatia<sup>5</sup>, Jennifer Johnson<sup>5</sup>, Alan Kuo<sup>5</sup>, Anna Lipzen<sup>5</sup>, Kerrie W. Barry<sup>5</sup>, Igor V. Grigoriev<sup>5,6</sup> & Connie Lovejoy<sup>2,3</sup>✉

Marine microbes that have for eons been adapted to stable salinity regimes are confronted with sudden decreases in salinity in the Arctic Ocean. The episodic freshening is increasing due to climate change with melting multi-year sea-ice and glaciers, greater inflows from rivers, and increased precipitation. To investigate algal responses to lowered salinity, we analyzed the responses and acclimatation over 24 h in a non-model Arctic marine alga (pelagophyte CCMP2097) following transfer to realistic lower salinities. Using RNA-seq transcriptomics, here we show rapid differentially expressed genes related to stress oxidative responses, proteins involved in the photosystem and circadian clock, and those affecting lipids and inorganic ions. After 24 h the pelagophyte adjusted to the lower salinity seen in the overexpression of genes associated with freezing resistance, cold adaptation, and salt tolerance. Overall, a suite of ancient widespread pathways is recruited enabling the species to adjust to the stress of rapid salinity change.

The Arctic Ocean is an ice-covered intercontinental ocean that is strongly influenced by seasonal melt cycles and fluctuations in salinity in the upper water column, as well as within and under sea-ice<sup>1</sup>. This puts the Arctic at the extreme end of an oceanic spectrum where water column temperature and salinity are identified as the strongest predictive factors for net production and structuring of microbial communities<sup>2–4</sup>. The extent and thickness of Arctic summer sea-ice has declined by more than 30% over the past four decades<sup>5</sup> and multi-year sea-ice is gradually being replaced by thinner first-year ice<sup>6,7</sup>. These changes are leading to more frequent inundations of fresher water onto the surface of seasonal ice, which is manifested by extensive melt pools<sup>8</sup>.

Arctic photosynthetic microalgae are at the base of the marine Arctic food web and support higher trophic levels across the Arctic Ocean. They inhabit the water column, but also live within and under sea-ice. The microalgae persist in ice-covered and ice-free summer waters near 0 °C and overwinter with no light in ice-covered waters below –1.5 °C<sup>9–11</sup>. Cryotolerant and cryophilic algae inhabit the water column and can tolerate salinity

fluctuations ranging from salinity 35 (seawater) to a minimum of salinity 3 during ice melt<sup>12</sup>. Over winter, they are found in sea-ice where temperatures can be much lower (<–15 °C), resulting in brine salinities exceeding 100 at the ice surface and over 40 at the underside surface<sup>13,14</sup>. The high salinity in sea-ice is due to brine channels that are produced during freeze-up when solutes are ejected from the ice, and salinity can increase drastically as salt becomes entrapped within the ice<sup>15</sup>. The brine persists into spring and even as air temperatures warm, salty pockets can appear near the surface of the ice. The constant transformations of Arctic sea-ice regimes impact biogeochemical cycles and ecological processes across trophic levels<sup>16</sup>, and algae both in the water column and those living in brine within ice are subjected to rapid changes in salinity. Synoptic studies suggest that Arctic microbes, including microalgae, carry genomic signatures and adaptations that enable them to live and function in this ice-influenced environment<sup>17,18</sup>. However, to date, only few polar algal species have been extensively studied genetically. These include the dinoflagellate *Polarella glacialis*<sup>19</sup>, Southern Ocean strains of the diatom *Fragilariopsis cylindrus*<sup>20,21</sup> and the haptophyte *Phaeocystis*

<sup>1</sup>Department of Natural Resource Sciences, McGill University, Ste. Anne-de-Bellevue, QC, Canada. <sup>2</sup>Institut de Biologie Intégrative et des Systèmes, Université Laval, Québec, QC, Canada. <sup>3</sup>Québec Océan, Département de Biologie, Université Laval, Québec, QC, Canada. <sup>4</sup>Centre d'Étude de la Forêt, Faculté de Foresterie, de Géographie et de Génomique, Université Laval, Québec, QC, Canada. <sup>5</sup>U.S. Department of Energy Joint Genome Institute, Lawrence Berkeley National Laboratory, Berkeley, CA, USA. <sup>6</sup>Department of Plant and Microbial Biology, University of California Berkeley, Berkeley, CA, USA.

✉ e-mail: [nastasia.freyria@mcgill.ca](mailto:nastasia.freyria@mcgill.ca); [Connie.Lovejoy@bio.ulaval.ca](mailto:Connie.Lovejoy@bio.ulaval.ca)

*antarctica*<sup>22</sup>, and four diverse Arctic flagellates (cryptophyte, haptophyte, ochromonad and pelagophyte)<sup>18,23</sup>. The four flagellates were originally isolated from Northern Baffin Bay at 77 °N, in the region commonly referred to as the North Water Polynya and by the Greenlandic-Inuktitut name *Pikialasorsuaq*.

Our study focuses on *Plocamiomonas psychrophila* Daugbjerg and Lovejoy, in the newly erected order Plocamiomonadales Daugbjerg and Lovejoy<sup>24</sup>. The strain (CCMP2097) was isolated from *Pikialasorsuaq*. *Plocamiomonas psychrophila* is a stramenopile in the algal class Pelagophyceae (Ochrophyta) and was originally isolated from a brine pocket on the surface of the sea-ice<sup>25</sup>. Although relatively less abundant in the Arctic compared to other nanoflagellates (2–20 µm cells), pelagophytes are persistently reported in Arctic 18S rRNA gene surveys, forming an evolutionarily distinct clade<sup>18</sup>. In tropical and temperate regions, the planktonic order Pelagomonadales are unicellular<sup>26</sup>, and several genera can cause large-scale algal blooms, commonly known as “brown tides”<sup>27,28</sup>. A second order Sarcinochrysidales tend to form colonies that are epibenthic or benthic<sup>29</sup>. Given the origin of the strain, we hypothesized that the alga would be adapted to fluctuating salinity, making it an ideal candidate to explore the transcriptomic responses to rapid salinity change. Several studies have demonstrated the presence of Pelagophyceae in the Arctic using 18S ribosomal RNA amplicon sequencing<sup>30–32</sup>, of which strain CCMP2097 is so far Arctic-specific<sup>11,18</sup>. Transcriptomic diversity in CCMP2097 was reported earlier from a study comparing high and low light regimes and use of organic versus inorganic nitrogen sources<sup>23,33</sup>. More recently, a study highlighted the genetic capacity of CCMP2097 to acclimate to a progressive decrease in salinity over a relatively long period (~34 days) over a range of salinities from 45 to 8<sup>25</sup>. Reducing salinity revealed specific metabolic pathways and the involvement of various proteins associated with hyper- and hypoosmotic shock, and the protective role of cold-responsive genes, such as antifreeze proteins. Antifreeze proteins are ice-binding or ice-structuring proteins (referred to as IBPs) that delay the recrystallization of water at

temperatures below –1.9 °C<sup>34</sup> and enable organisms to adapt and survive in sub-zero environments<sup>35</sup>.

Salinity is a stress that can impact the physiological and biochemical pathways of microorganisms, potentially hindering their growth and survival. However, in extreme environments, many organisms, including microalgae, can adjust their metabolism to adapt to a change in salinity<sup>36,37</sup>. In line with the findings of Freyria, et al.<sup>25</sup>, we hypothesized that stress-sensitive genes would be generally expressed in this arctic strain in response to rapid freshening. To test this hypothesis, we conducted experiments in which CCMP2097 was transferred to media adjusted to salinities of 16 or 22, which occur just below melting ice<sup>1</sup>. The algae were monitored over 24 h after transfer for cell viability and nutrient uptake response. RNA-seq was applied to identify up and down regulated genes over the same time period. Comparative transcriptomics revealed a plethora of oxidative stress-response genes, as well as some circadian genes expressed in Pelagophyte CCMP2097 involved in the rapid acclimation of the microalga to sudden change of salinity. We show overexpression of freezing resistance, cold acclimatization, and salt stress tolerance genes. The results suggest multiple strategies are used by polar marine microalgae to persist in a highly variable saline environment and are entwined with evolved mechanisms used to protect cells exposed to multiple environmental stresses.

## Results

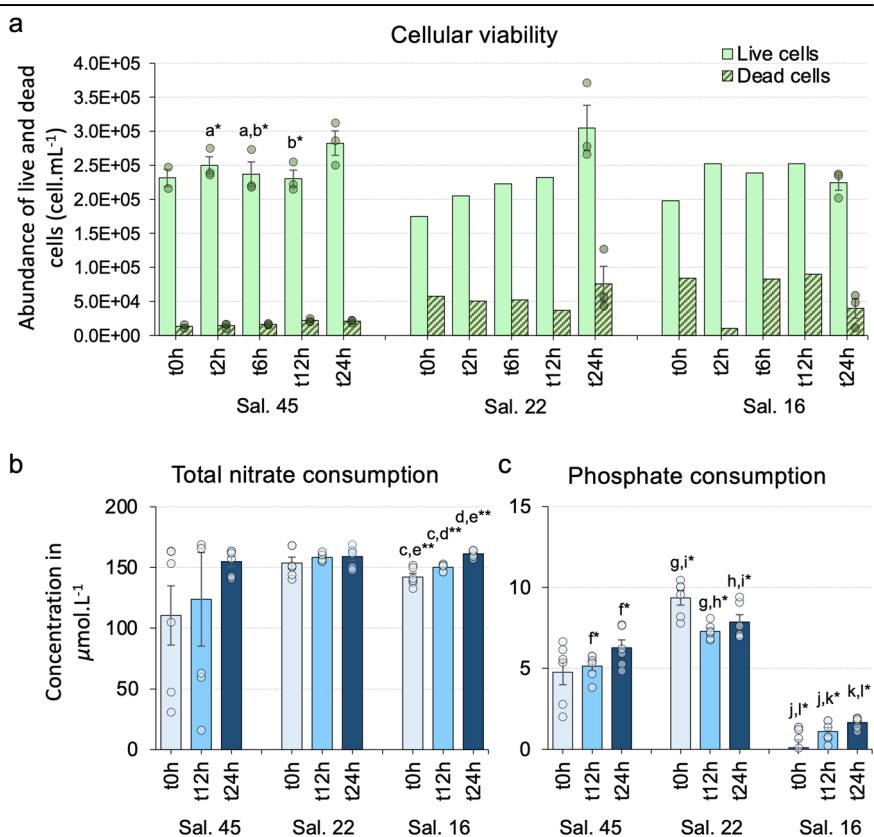
We exposed the microalga to a sudden salinity (Sal.) change, and measured transcriptional gene expression at 0, 2, 6, 12 and 24 h after transfer to a lower salinity. We compared this to transcriptomes following transfer to new media with the same initial salinity (Supplementary Fig. S1a,b).

### High initial cell death at lower salinities followed by recovery and nitrate uptake

We monitored cell viability after each harvest using a live-dead fluorescent stain and flow cytometry after exposure to lower salinities (Fig. 1 a). For the control condition at Sal.45, the dead cell proportions were consistently low,

**Fig. 1 | Cell health and nutrient consumption.**

**a** Cellular viability with concentration of live and dead cells.mL<sup>-1</sup> at the time of sampling. Error bars of live and dead cells include triplicate values (*n* = 3). **b, c** Nutrient (total nitrate and phosphate) consumptions at the time of sampling. Error bars are for the triplicate cultures with biological replicates (*n* = 6). Standard deviation was used to calculate error bars. Missing error bars mean that triplicate values were not available. Letters “a” to “l” refer to two-way ANOVA tests for cellular viability and nutrient consumption (Supplementary Tables S2 and S4). Only significant *p* values (<0.05 \* and <0.01 \*\*) are shown.



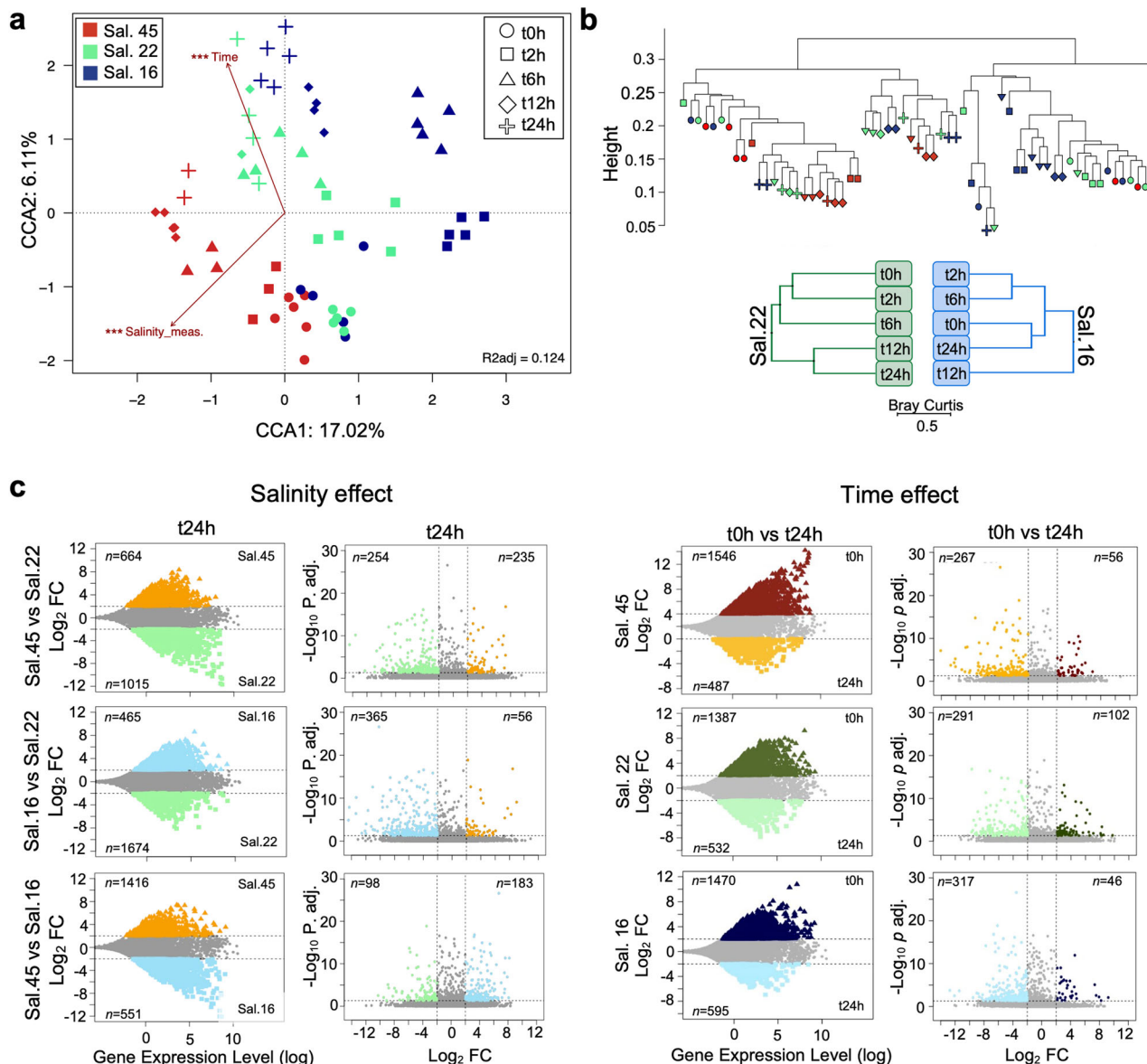


**Fig. 2 | Clustering of transcriptome samples.** **a** Canonical Correspondence Analysis (CCA) with the Bray-Curtis dissimilarity measure of reads per gene of all transcriptomes. Arrows indicate time of sampling and actual salinity measured at each time of sampling. **b** Hierarchical clustering of all samples based on normalized reads and Unweighted Pair Group Method with Arithmetic Mean (UPGMA) based on the Bray-Curtis distance matrices of significant DEGs of salinity 16 and 22 for all sampling times. **c** Scatter plots show the comparison between salinities for the time

of sampling t24h (left panels—salinity effect) and between t0h versus t24h for each salinity (right panels – time effect). Right panels show scatter plot. Each point represents a unigene. Points greater than 2 of  $\text{log}_2$  Fold Change (FC) indicate up-regulated genes and lower than  $-2$  indicate down-regulated genes. Color points indicate differential expressed genes (DEGs). Right panel shows volcano plots of comparison between t0h versus t24h for each salinity condition. Color points indicate only filtered DEGs with an adjusted  $p$  value  $< 0.05$ .

not exceeding 8.9% of all triplicates (Supplementary Table S1). Significant differences were observed in the number of live cells between t2h and t6h, as well as between t6h and t12h (ANOVA,  $p$  value  $< 0.05$ ; Supplementary Table S2) with replication between the independent flasks. However, due to logistical constraints, only a single replicate was sampled at each time point for Sal.16 and 22, except for t24h. The proportion of dead cells for Sal.22 was found to be about three times that of the control values, and four times for Sal.16. The t24h data from all three replicates showed greater variability compared to the control. Cultures at Sal.16 had a maximum proportion of 33.1% dead cells, while at Sal.22 it was of 31.3% dead cells (Supplementary Table S1 and Fig. 1a).

Nutrient concentrations were measured for each condition at t0h, t12h and t24h (Supplementary Table S3), yielding nutrient consumption data. The highest total nitrate consumption by cells was at t24h for all salinities,

and significant differences were noted between t0h-t12h, t12h-t24h and t0h-t24h for Sal.16 only (ANOVA,  $p$  value  $< 0.05$ ; Fig. 1b and Supplementary Table S4). Cells consumed more phosphate over 24h at Sal.22 but plummeted at Sal.16. Significant differences in phosphate were found for all salinity conditions over time (ANOVA,  $p$ -value  $< 0.05$ ; Fig. 1b and Supplementary Table S4).

### Differential gene expression over time under lowered salinity

Canonical correspondence analysis (CCA) was performed using all conditions and sampling times. The results showed a clear separation of samples based on salinity along the first axis, while the second axis indicated a separation of samples based on the time of sampling (Fig. 2a). The CCA ordination demonstrated statistical significance (ANOVA:  $F = 5.48$ ,  $p$  value  $< 0.001$ ). Most of the cells of all salinities at t0h clustered

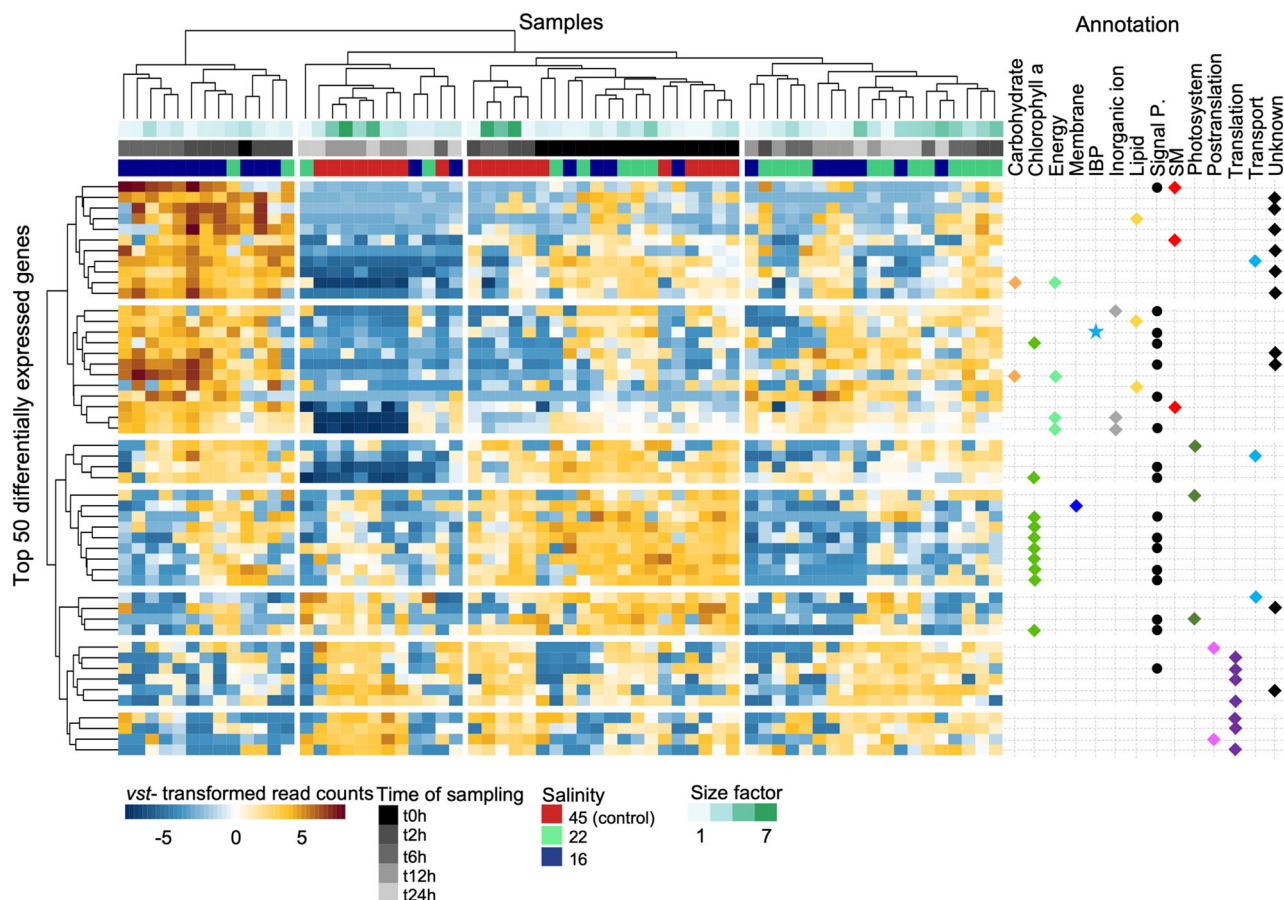


**Fig. 3 | Top 50 differentially expressed genes of the pelagophyte CCMP2097.** Heatmap of clustered results based on normalized and transformed read counts. The functional annotation of each gene is on the right of the heatmap, indicated by diamonds, with each category having a separate color. Note that unknown function genes are indicated as black diamonds. Genes with signal peptides are indicated by

filled black circles. The variance stabilizing transformation (*vst*) is calculated with the *vst()* function within the *DeSeq2* package on R and transforms the count data to normalize the read count. Size factor corresponds to the sequencing depths of each transcriptome. Acronyms: IBP ice-binding protein, Signal P. signal peptide, and SM secondary metabolites.

together, with samples at t2h for the control samples (Sal.45). Sal.22 samples were grouped around the center of the ordination. The culture condition variables, including the salinity measured at each time and the time of sampling, were significant ( $R^2 = 1$ ,  $p$  value < 0.001). The same treatment clustering pattern emerged using the dendrogram constructed using the complete linkage method on normalized reads of all samples for each condition, indicated that the later times of sampling clustered apart from earlier times (Fig. 2b). An unweighted pair group method with arithmetic mean (UPGMA) tree indicated proximity between samples from Sal.16 and 22 (Fig. 2b).

Through our analysis, we identified differentially expressed genes (DEGs) across all salinities over time (salinity effect) and all sampling times at each salinity (time effect; Fig. 2c). In comparing the salinity effects, we observed the highest number of DEGs (3161) at t2h at Sal.16 compared to t2h at Sal.45. Conversely, the lowest number of DEGs (411) were detected in the same comparison at t2h at Sal.45 compared to t2h at Sal.16 (Supplementary Fig. S2). When comparing the time effect, the highest number of DEGs (2247) was detected at t6h compared to t12h at Sal.22, while the lowest number of DEGs (471) was found at t12h compared to t6h at Sal.16 (Supplementary Fig. S3). For both sets of comparison (salinity and time effects), volcano plots show the significant DEGs (defined as DEGs with a  $p$  value < 0.05), this stringency reduces the number of DEGs considered (Fig. 2c and Supplementary Figs. S2, S3). To separate the net effect of salinity from the effect of time, we compared and identified significant DEGs in all conditions. We then removed the significant DEGs detected in the Sal.45 control samples that were also detected at lower salinities, as these would not

be determined by the salinity treatment but presumably due other factors that were not measured.

### Functional potentials in the pelagophyte

As part of our initial inspection of all genes, we identified the “top” 50 most variant DEGs in all samples based on normalized and transformed read counts (Fig. 3). Based on expressed genes, samples separated into 7 vertically arranged gene centric clusters. Across these clusters, the majority of t6h time point Sal.16 samples grouped together in the 1st major cluster, while the second group consisted mostly of early time point Sal.45 samples. The 3rd group comprised later time points mostly at t24h from the three conditions. The samples in the 4<sup>th</sup> group were taken from the initial and early lower salinities (16 and 22) of t0h and t2h. Within the functional annotation for the top 50 most variant DEGs, we observed DEGs annotated as chlorophyll *a* binding protein and for photosystem proteins among t0h samples. Only one DEG was annotated as an ice-binding protein (IBP, pfam11999) with a signal peptide, which corresponds to an extension of the amino acid sequence indicating where the protein is destined to be transported inside or outside the cell<sup>38</sup>. Lastly, two clusters consisted mostly of DEGs annotated in the “Translation” and “Post-translation” categories (Fig. 3).

By mapping all transcriptomes onto the CCMP2097 reference genome<sup>18,39</sup>, we retrieved the functional annotations of genes from the Kyoto Encyclopedia of Genes and Genomes ontology (KEGG; Fig. 4a) pathways. DEGs annotated under the class “Metabolism of complex carbohydrate” and “Carbohydrate” and “Energy” metabolisms were more prevalent in Sal.16 at all times of sampling compared to higher salinities. Functional





**Fig. 4 | KEGG and KOG pathways for each condition of salinity between time of sampling.** **a** KEGG pathway annotation among all differential expressed genes (DEGs). **b** KOG pathway annotation among all DEGs. The number of DEG is indicated by the size of the dots.

annotation from the Clusters of Orthologous Groups of proteins (KOG/COG) database revealed DEGs encoding the categories “Replication, recombination and repair”, “RNA processing and modification”, and “Posttranslational modification, protein turnover, chaperones”, which were predominantly observed for lower salinities over time (Fig. 4b). The Gene Ontology (GO) terms provide functional annotation of gene products in three domains: Biological Processes (BP), Cellular Components (CC), and Molecular Function (MF). In the BP domain, Sal.22 and 45 had higher numbers of DEGs annotated (ca. 5 genes) within “electron transport” and within “metabolic process” (ca. 15 genes; Supplementary Fig. S4). In the CC domain, under all salinity conditions, a maximum of 8 DEGs encode for “membrane” and about 6 DEGs encode for “nucleus” (Supplementary Fig. S5). In the MF domain, the DEGs were annotated in several enzyme families ranging from “amidase” to “transferase”. A complete list of enzyme families is given in Supplementary Fig. S6.

### Co-expression network of significant DEGs

We analyzed the expression patterns of all 607 significant DEGs (with a  $p$  value  $< 0.05$ ) that were detected in all transcriptomes. This analysis was performed using the weighted gene co-expression network analysis (WGCNA; Fig. 5). Based on the similarity of gene expression, the WGCNA classified all DEGs into 8 modules (Fig. 5a). Multiple modules exhibited positive or negative correlation with specific sampling times and salinity conditions (Fig. 5b). Four modules were found to be significantly positively

correlated (Turquoise:  $p$  value  $< 0.05$ ; Black:  $p$  value  $< 0.01$ ; Blue and Brown:  $p$  value  $< 0.001$ ) with the Sal.16. The Blue and Brown modules show a significant positive correlation with t2h, but a significant negative correlation with Sal.45. We selected Black, Blue, and Brown modules with the highest  $p$  values to investigate interactions between specific DEGs. The black module displayed an interaction between 20 DEGs, with one encoding for an aluminum-activated malate transporter (ALMT, pfam11744) representing the hub gene corresponding to the highest correlation and highest connectivity in the network module (Supplementary Fig. S7). The Blue and Brown modules contained 65 and 40 DEGs, respectively (Fig. 5b), and both hub genes have no known functions (Supplementary Figs. S8, S9).

### Significant DEGs in the cell suggest interacting processes

A total of 607 significant DEGs were identified. Of these, 188 were selected for further analysis. This was done by exploiting the results of module networks (Supplementary Figs. S7, S9) and exploring functional annotations. In a schematic diagram of the pelagophyte cell, we provide a summary of the potential roles and implications of the selected DEGs in the response of the pelagophyte exposed to rapid decrease in salinity (Fig. 6).

### Compatible solute and osmoprotection

We identified eleven DEGs encoding proteins associated with osmotic regulation, osmo-protection, osmolyte synthesis, or transport of osmolytes within the cell (Figs. 6, 7 and Supplementary Figs. S10, S11). One of these

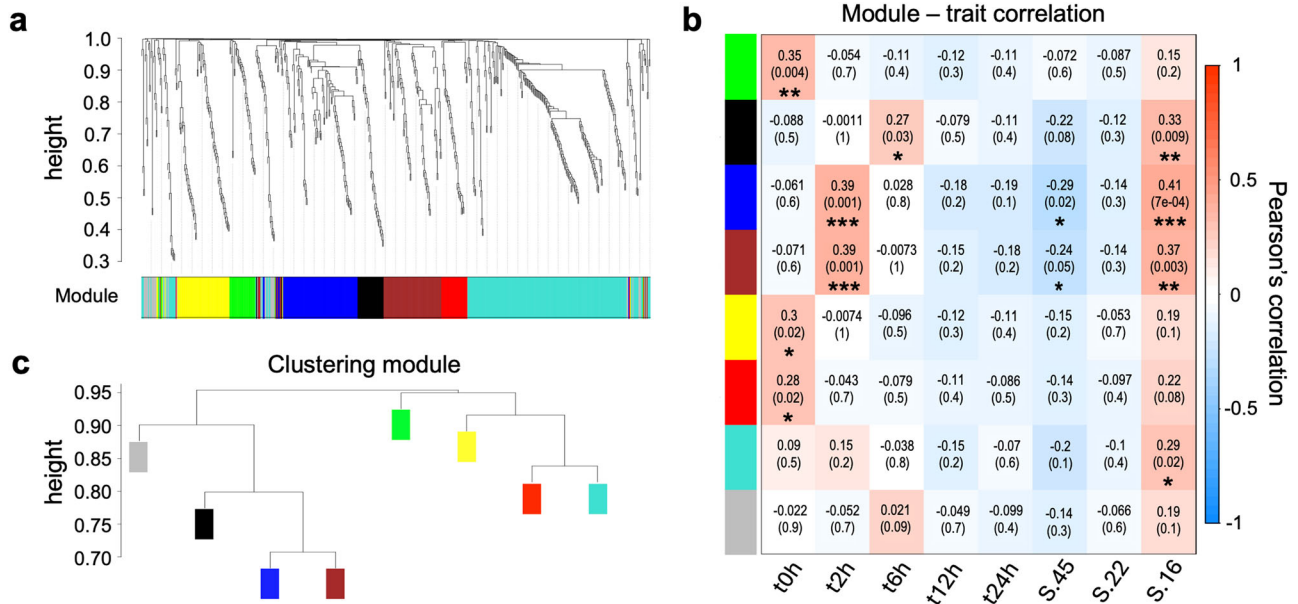


**Fig. 5 | Weighted gene co-expression Network Analysis of differentially expressed genes (DEGs).** **a** The dendrogram plot represents each DEGs that clustered into 8 color modules, represented by the bar color module at the bottom of the dendrogram. Genes were clustered based on a dissimilarity measure (1-TOM). **b** Module with weighted correlations and corresponding *p*-values at time of sampling, and

salinity conditions. The color scale shows module-trait correlation based on Pearson’s rank correlation. Asterisks within the correlation indicate the significance level *p* value from Pearson’s *Rho* (*p* value < 0.05\*, < 0.01\*\* and < 0.001\*\*\*). **c** The module network dendrogram was constructed by clustering module eigengene distances.

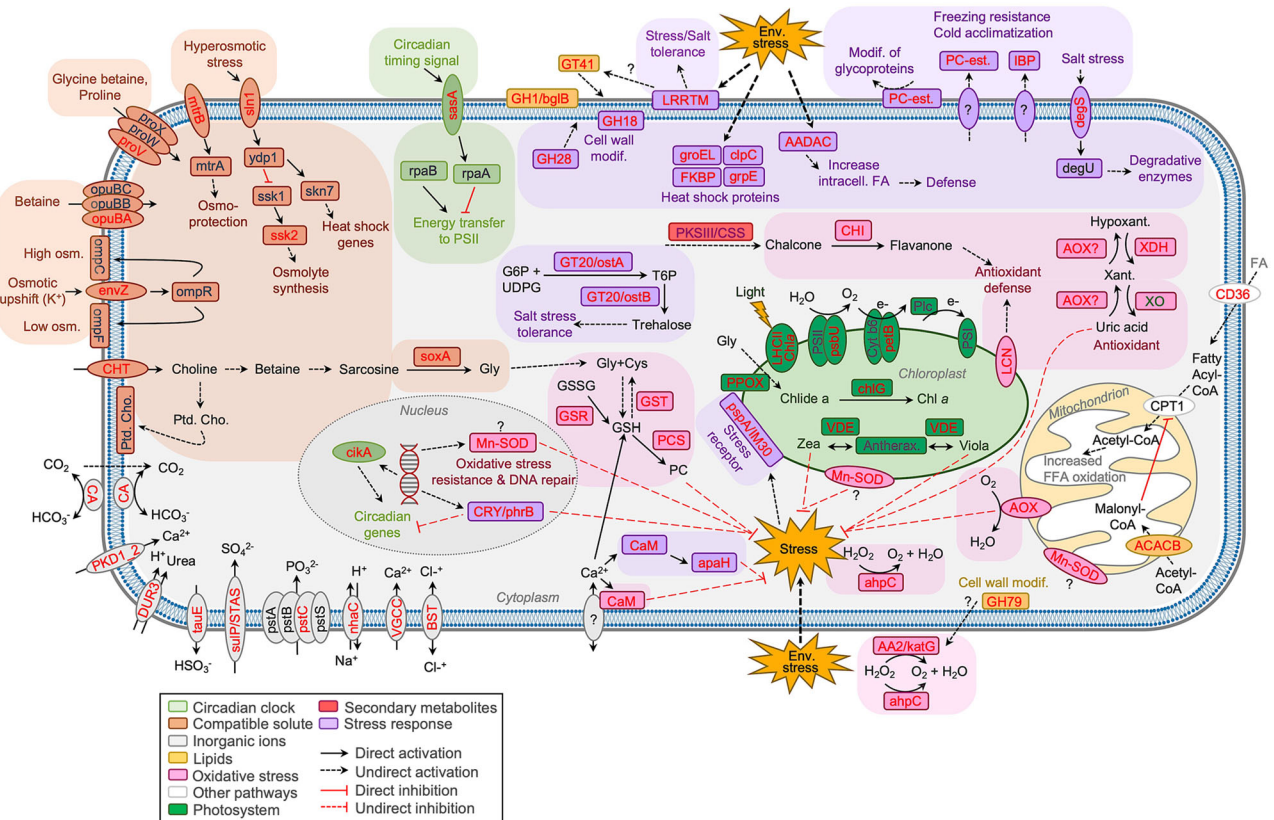


**Fig. 6 | Schematic representation of the pelagophyte *Placamiomonas psychrophila* CCMP2097 metabolic system based on the 188 selected significant differentially expressed genes.** The presence of the gene in the transcriptomes are denoted

by red text. Gene background color indicates the metabolic category. A complete list of genes and annotations can be found in Supplementary Data 1. Figure created entirely with Microsoft PowerPoint v.16.88.



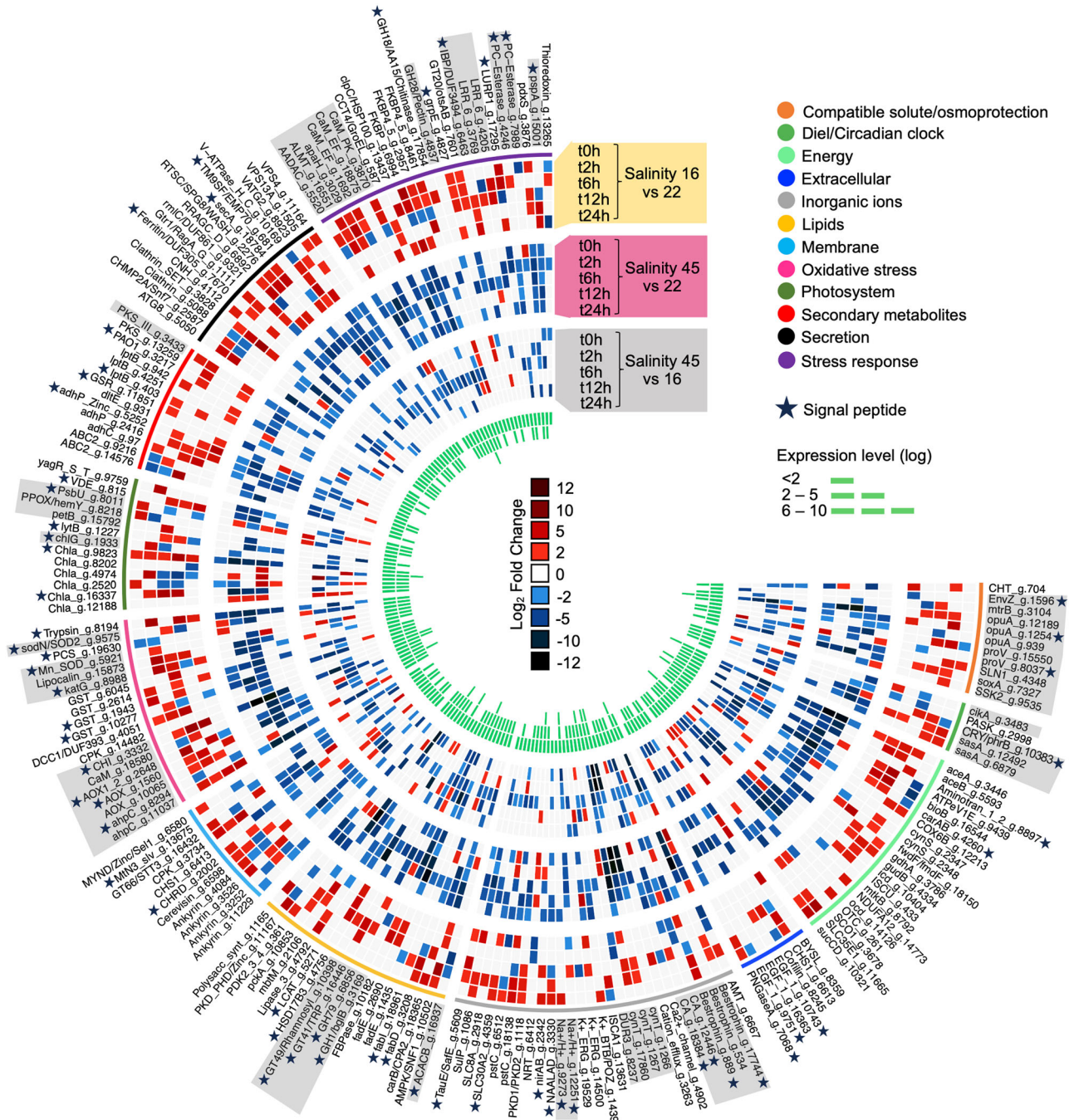


**Fig. 7 | Circular heatmap of 188 selected differentially expressed genes and their expression profile based on the log<sub>2</sub> fold change for salinity effect. Values of up-regulated DEGs are indicated by shades of red and down-regulated DEGs by shades**

of blue. Colors in the outer circle indicate metabolic categories for each DEG. Gray boxes highlight DEG described in the main text. A complete list of genes and annotations can be found in Supplementary Data 1.

DEGs encodes a sensor histidine kinase, *mtrB*, and belongs to a two-component system. This gene demonstrated expression at later sampling times (t6h to t24h at Sal.16 and t12h to t24h at Sal.45; Supplementary Fig. S10) and predominantly at Sal.16 compared to Sal.22 and Sal.45 (Fig. 7). Another DEG from the two-component system is *envZ* that has a signal peptide. Upregulation of *envZ* gene was observed only at lower salinities (t24h at Sal.16 and 22; Fig. 7 and Supplementary Fig. S10). *EnvZ* encodes for an inner-membrane histidine kinase that functions as an osmolarity sensor and can respond to various external stimuli such as osmotic pressure, temperature, or pH by phosphorylating the protein *ompR* and acting on two transmembrane proteins (*ompC* or *ompF*) depending on the external osmolarity and nutrient availability<sup>40</sup>. Another osmolarity sensor, *sln1* gene

was upregulated only at lower salinities, mostly at earlier sampling times (Fig. 7 and Supplementary Fig. S10). Following *sln1* regulation, an osmosensing MAP kinase cascade can be activated<sup>41</sup>. Cells exposed to high salinity that have sufficient osmolytes to act as an osmoprotectant, can activate the cytoplasmic response regulator encoded by *ssk2* gene (Fig. 6).

Furthermore, we identified seven DEGs involved in osmolyte transport inside the cell. The *soxA* gene encodes a sarcosine oxidase, a choline transporter protein responsible for converting intracellular choline into betaine and sarcosine, which can be further degraded into glycine. The *soxA* gene was upregulated at lower salinities between t6h to t24h (Fig. 7). Three DEGs annotated as *opuA* encodes an osmoprotectant transmembrane transporter. Among the three DEGs, one possesses a signal peptide, and

another was highly expressed at lower salinities (Supplementary Data 1) with a high gene expression level (>6 log; Fig. 7). The OpuA transporter imports betaine into cells and provides a high degree of osmotic tolerance<sup>42</sup>. Additionally, the *proV* gene encodes for a mineral and organic ion ABC transporter that can transport glycine, betaine, and proline. *ProV* was expressed in all salinities, but more so at lower salinities (Fig. 7) and was identified as the hub gene in the Blue module network (Supplementary Fig. S8).

### Circadian clock

Five differentially expressed genes (DEGs) encoding proteins involved in circadian clock regulation were identified (Fig. 7, Supplementary Figs. S10, S11 and Supplementary Data 1). Three genes encode components of a two-component system, consisting of a transmembrane sensor and a cytoplasmic response regulator (Fig. 6). *SasA* gene encodes a clock-associated kinase, was mostly upregulated at Sal.16 and Sal.22 (Fig. 7 and Supplementary Fig. S10). However, *cikA* gene, a sensor histidine kinase, was mostly upregulated Sal.22 at earlier time points. The two-component system proteins (*sasA* and *cikA*) may activate circadian genes, while the stress-response protein encoded by the *CRY/phrB* gene inactivates circadian genes (Fig. 6). The *CRY/phrB* gene belongs to the cryptochrome photolyase protein family (CPF) and possesses a signal peptide. This CRY gene was upregulated from t0h to t6h at both lower salinities, with no overexpression at Sal.45 versus Sal.16 (Fig. 7).

### Cold-resistance gene expression

Three genes were identified within the “Stress response” category: one encoding for an IBP and two encoding a PC-Esterase. Although CCMP2097 genome contains ten genes encoding IBPs, our data indicated that the one overexpressed IBP gene had a signal peptide and was upregulated mostly at later time points (t6h to t24h) at both lower salinities (Fig. 7). The pelagophyte CCMP2097 genome possesses nine genes encoding a PC-esterase, but only two PC-esterase genes, both with a signal peptide, were upregulated: gene\_4246 was upregulated mostly at Sal.22 throughout the 24 h, while gene\_7989 was overexpressed earlier (t0h and t2h) for both lower salinities (Fig. 7).

### Inorganic ion uptake regulation

Within the “inorganic ions” category, two DEGs had the highest number of reads per gene (Supplementary Fig. S11), one encoding a urea proton symporter (DUR3), and the second encoding a sodium/hydrogen (Na<sup>+</sup>/H<sup>+</sup>) symporter (Supplementary Data 1). Additionally, five DEGs encode for proteins carbonic anhydrase (*CA* and *cynT*), which are key enzymes actively involved in photosynthetic CO<sub>2</sub> fixation, catalyzing the reversible reaction of CO<sub>2</sub> hydration to bicarbonate HCO<sub>3</sub><sup>-</sup>.<sup>43</sup> In addition, three other DEGs encoded a bestrophin chloride channel (BST). Two genes possess a signal peptide, indicating its potential to encode an outer membrane protein, while a third lacks a signal peptide and may encode the inner membrane protein transporter (Fig. 6 and Supplementary Data 1). The two DEGs possessed a signal peptide and were more expressed with a higher gene expression level at lower salinities (Fig. 7).

### Lipid dynamics

Among the twenty DEGs involved in the “lipids” category, six have a signal peptide and four belong to carbohydrate-active enzymes (cazyme) family (Figs. 6, 7 and Supplementary Figs. S10, S11). Within the glycosyl hydrolase (GH) and glycosyltransferase (GT) family, numerous cazymes play a role in lipid/fatty acid (FA) biosynthesis, metabolism and/or degradation. Additionally, we identified four DEGs with a signal peptide that are involved in cell wall modification: a beta-glucosidase, GH1/bglB; a beta-glucuronidase, GH79; a peptide N-beta-glucosyltransferase, GT41; and a rhamnosyl transferase, GT49 (Figs. 6, 7, Supplementary Figs. S10, S11 and Supplementary Data 1). Furthermore, an acetyl-CoA/biotin carboxylase (ACACB) that possesses a signal peptide was upregulated at t2h to t6h at Sal.16 and at t12h at Sal.45 (Fig. 7). ACACB removes the inhibitory effect on a carnitine

O-palmitoyltransferase CPT1, leading to increased FA oxidation (Fig. 6). The transmembrane glycoprotein CD36 may facilitate cellular long-chain FA uptake across the cell membrane<sup>44</sup>, which may also lead to increased FA oxidation.

### Oxidative stress genes and cell defense

Numerous antioxidant and defense responses of the pelagophyte were expressed (Figs. 6, 7 and Supplementary Figs. S10, S11). For instance, the generation of uric acid by the specific enzyme xanthine dehydrogenase, and the action of flavanone by modifying chalcone through the chalcone/flavanone isomerase (CHI) converting chalcone to flavanone. The aforementioned enzymes are potentially involved in antioxidant responses. Of the 19 DEGs categorized under “oxidative stress”, 10 have a signal peptide and three encode for alternative oxidase (AOX). Moreover, one DEG encodes for a lipocalin (LCN), also known as cytosolic FA binding protein, which is a transporter of small hydrophobic molecules such as lipids. This gene was upregulated mainly between t2h to t12h at both lower salinities (Fig. 7). Furthermore, we identified two DEGs with a signal peptide encoding for a Mn-superoxide dismutase with Mn<sup>2+</sup> as cofactor (Mn\_SOD). Both genes were upregulated at Sal.16 but not simultaneously, one at t2h (Mn\_SOD) and at t6h (sodN/SOD2; Fig. 7).

The only auxiliary activity (AA) identified among the cazyme within the significant DEGs was AA2, a catalase-peroxidase (katG) with a signal peptide. Through the WGCNA Brown module network, we discovered that the previously mentioned GH79 was directly related to katG (Supplementary Fig. S9). KatG and the enzyme alkylhydroperoxyreductase (*ahpC*) are induced in response to oxidative stress<sup>45</sup>. Of the two DEGs annotated *ahpC*, one has a signal peptide (Supplementary Data 1), but both DEGs were mainly upregulated at Sal.22 over time (Fig. 7). Another antioxidant protein observed was the calmodulin Ca<sup>2+</sup> binding sensor (CaM) with an enkurin domain. CaM-Ca<sup>2+</sup> was upregulated only between t2h to t6h at both lower salinities (Fig. 7).

### Photosystem and pigments

Among the “photosystem and pigment related proteins”, we identified six DEGs encoding a chlorophyll *a* binding protein (Fig. 7 and Supplementary Figs. S10, S11). In addition, two genes were upregulated, *petB* and *psbU*, which are involved in the PSII system. PetB is a cytochrome b6 that receives electrons from PSII and transfers them to plastocyanin (Plc) and ultimately to PSI for energy<sup>46</sup> (Fig. 6). The *psbU* protein possesses the ability to bind manganese (Mn<sup>2+</sup>) and plays a role in optimizing calcium (Ca<sup>2+</sup>) and chloride (Cl<sup>-</sup>) binding affinities for water oxidation<sup>47</sup>. Additionally, we identified two DEGs involved in the chlorophyll biosynthesis pathway. The *hemY* gene contains a signal peptide and functions as a protoporphyrinogen oxidase in the porphyrin metabolism. *HemY* encodes the PPOX enzyme, which catalyzes the conversion of protoporphyrinogen to protoporphyrin. In photosynthetic organisms, protoporphyrin is finally converted to chlorophyllide *a*, which is further converted to chlorophyll *a* by chlG. The *chlG* gene was mainly upregulated at t2h to t6h at lower salinities (Fig. 7 and Supplementary Data 1).

### Secondary metabolites

Within the “secondary metabolites” category, we identified a polyketide synthase III (PKSIII/CSS) a backbone gene encoding a chalcone/stilbene synthase, also known as CHS/STS. The PKSIII enzyme has an important role in flavonoid and pigment biosynthesis and its products exhibit antioxidant activity<sup>48</sup>. The PKSIII gene was upregulated mostly at lower salinities both at t0h to t2h and t24h (Fig. 7). However, a differential expression was observed for this gene at sal.45 at t12h.

### Other stress-response genes

Within the “Stress response” category, we identified three additional DEGs encoding CaM that were mainly upregulated between t0h to t6h at lower salinities (Fig. 7). Two DEGs encode a CaM with an EF-hand binding domain, while another encodes a CaM dependent on a protein kinase (PK)



activity (Fig. 6 and Supplementary Data 1). The CaM-PK can activate a  $\text{Ca}^{2+}$ -dependent calcineurin phosphatase (apaH), which is regulated by intracellular  $\text{Ca}^{2+}$  levels and acts as a signaling intermediate<sup>49,50</sup>. *ApaH* gene expression was upregulated between t0h to t6h at Sal.16 when compared to Sal.22, and potentially inhibits further generation of intracellular reactive oxygen species (ROS)<sup>51</sup>.

Our analysis identified various DEGs encoding environmental stress-response proteins, notably, a gene encoding for an arylcetamide deacetylase (AADAC) that was only upregulated at lower salinities (Fig. 7 and Supplementary Fig. S10). AADAC facilitates the increase of FA in the cell as a defense mechanism<sup>52</sup>. Furthermore, the gene encoding for a membrane chaperone, (*pspA/IM30*), and was upregulated at all sampling times at Sal.22 (Fig. 7). The *pspA* protein, also known as IM30 in eukaryotes, acts as a membrane stress receptor<sup>53</sup>. Additionally, we found other DEGs encoding a chitinase (GH18), and the GH18 gene was only upregulated at t2h at both lower salinities (Fig. 7 and Supplementary Fig. S10). Similarly, GH28 gene was upregulated only at lower salinities at t0h and t24h and is a polygalacturonase linked to a pectin lyase. Finally, we found two DEGs encoding a leucine-rich repeat transmembrane protein (LRR), and both DEGs were mainly upregulated at lower salinities (Fig. 7). LRR had a direct connection in the Brown module network with the previously mentioned GT41 (Supplementary Fig. S9).

## Discussion

Our experimental transcriptomic analysis revealed a plethora of stress resistance, and tolerance genes expressed in *P. psychrophila* CCMP2097 when exposed to rapid salinity reduction over 24h. Our previous study of CCMP2097 investigated the transcriptomes associated with growth under a progressive range (45 to 8) of salinities over a month and highlighted the expression of specific cold-resistant proteins, such as IBP and PC-esterase<sup>25</sup>. Interestingly, none of the 3 IBPs genes and 2 PC-esterase genes expressed in the long-term study were upregulated in the present study. In contrast, a single gene coding for IBP and the two genes coding for PC-esterase were differentially expressed in this study, and were different from DEGs observed Freyria, et al.<sup>25</sup>. The differences between the short-term, more immediate response and the expression profiles after acclimation of these cold-resistance genes<sup>25</sup> indicate the use of distinct mechanisms enabling the alga to adjust to a variable unpredictable environment where both rapid and slower salinity changes could occur. In the two experiments (this study and Freyria, et al.<sup>25</sup>) only ca. half of the IBP and PC-esterase genes (10 and 9 genes, respectively) in the genome of CCMP2097 were differentially expressed, and triggers for gene expression in the remaining IBPs and PC-esterase genes are unknown. The multiple IBP genes in the *Plocamiomonas* and other endemic polar eukaryotic microalgae<sup>18</sup> is in keeping with the diversity of multiple actions of IBPs in ice-influenced environments<sup>54</sup>. The diversity provides a suite of potential tools to respond to environmental conditions and even modify the immediate environment<sup>54</sup>.

In our alga, cells appeared stressed at t0h, coinciding with the media change and the number of dead cells observed, regardless of the salinity (Fig. 1a and Supplementary Table S1). Salinity stress can accelerate nutrient uptake in higher plants<sup>55,56</sup>. However, the alga only consumed more nutrients at t24h than at the earlier time points (Fig. 1b, c and Supplementary Table S3), suggesting nutrient uptake as indication of acclimation to the new conditions and the start of active growth. The discrepancy between nitrate uptake or consumption compared to phosphate under the varying conditions is consistent with multiple nitrate transporters in the pelagophyte<sup>23</sup>, which would be required under nitrogen limiting conditions that prevail over the Arctic<sup>57</sup>, and by way of contrast the phosphate transporters are much less diverse.

The onset of growth and dependence on photosynthesis was also indicated by the overexpression of a transporter in bestrophin chloride channel (Fig. 7 and Supplementary Fig. S10). In some plant species, a bestrophin-like protein plays a role in adjusting photosynthetic light utilization in electron transport and photoprotection mechanisms<sup>58</sup>. In this case CCMP2097 demonstrated swift ion balance adjustments within cells, in

response to external changes (here salinity), which would be analogous to reports of cells regulating ion transport in the chloroplast to adapt to variable light<sup>59</sup>. The link between ion transport regulation and photosynthesis requires further investigation in euryhaline algae, which tend to be exposed to cyclic salinity conditions.

Generally, the top 50 DEGs indicate that cells in the t0h samples expressed proteins involved in energy production, such as those involved in photosystem and pigmentation, and proteins related to translation, lipid biosynthesis or degradation, and inorganic ion transport (Fig. 3). These findings were consistent with cells expressing coding genes that contribute to maintaining cell health and energy acquisition when exposed to novel conditions. The pelagophyte appeared to require rapid regulation of its energy demand through photosynthesis and pigment biosynthesis. This was achieved through different proteins, such as chlorophyll *a* binding protein and carotenoids, which are fat-soluble pigments<sup>60</sup>. These pigments can accept electrons from reactive species to neutralize free radicals in the cells<sup>61</sup>. This would be crucial to quickly adjust to new conditions and contribute to overall plasticity. Moreover, the pelagophyte regulated energy demand in response to low salinity by increasing  $\beta$ -oxidation of FA in the mitochondrion (Fig. 6). This leads to the production of more molecules of acetyl-CoA, which can be utilized as an energy source in the Krebs cycle<sup>62</sup>.

Additionally, the importance of the CRY/phrB protein (circadian genes), belonging to the cryptochrome/photolyase protein family (CPF) and was previously detected in the green alga *Chlamydomonas reinhardtii*<sup>63</sup>, lies in its overexpression at low salinity between early time of sampling (t0h to t6h; Fig. 7). This protein is thought to function as a circadian photoreceptor and has a role in DNA repair and transcriptional regulation<sup>64</sup>. In *Synechococcus elongatus*, the circadian clock is reset by a phytochrome-like histidine protein kinase by external signals from the environment, including light and temperature<sup>65</sup>. Similar to plants like *Arabidopsis thaliana*, cryptochromes and phytochromes work synergistically to receive clock-setting information<sup>66</sup>. Coesel, et al.<sup>67</sup> observed diel oscillations in several open-ocean eukaryotic plankton communities, which included Pelagophyceae. These oscillations are entrained through the activity of light-sensitive photoreceptors of the cryptochrome/photolyase family. This mechanism enables organisms to respond promptly to variations in light exposure. It appears that in CCMP2097, an abrupt change in salinity can serve as a clock-setting signal to reset circadian clock genes and aid the cell to adapt to its new environment. This adaptation in Arctic algae may be related to greater ice melt during mid-day and could have evolutionary implications.

Marine microalgae in the Arctic sea ice-influenced ecosystem face the challenge of coping with a highly variable saline environment. The *mtrB* gene, encodes a protein that offers protection against high salinity, heat, and cold stress<sup>68,69</sup>. For the pelagophyte, this gene can be triggered when encountering lower salinity or a change in osmolarity in the environment (Fig. 6). A sudden change in salinity triggers an automatic osmotic adjustment of the cell wall, facilitated by the activation of multiple inorganic ion transporters. In the pelagophyte, the expression of the sodium/hydrogen symporter was upregulated under low salinity conditions (Fig. 7). Sodium ion transport across the cell membrane is critical for maintaining osmotic balance and facilitating effective cellular adaptation to external changes<sup>70</sup>. The maintenance of osmotic balance is supported by compatible solutes. The pelagophyte expresses the *proV* gene encoding a transporter for glycine, betaine, and proline. This transporter is favored when sufficient osmoprotectants are present in the cell's surroundings<sup>71</sup>.

The diverse genes expressed in the pelagophyte suggest the acquisition of multiple protective strategies against stressors like ROS, which are normal by-products of aerobic metabolism and play a role in several different pathways<sup>72</sup>. This includes signal transduction, activation cascades, transcription, and gene expression. Environmental stresses, such as cold, and high-intensity light, increase photosynthetic oxidative stress and the production of ROS, as observed in the red alga *Cyanidioschyzon merolae*<sup>73</sup>. To alleviate oxidative stress, microalgae employ mechanisms through enzymes such as CA, which is essential for  $\text{CO}_2$  fixation during photosynthesis, as

well as antioxidant and scavenging enzymes. The antioxidant system can be rapidly activated by the expression of stress-responsive genes, as observed in the green alga *Dunaliella salina*, after exposure to salt stress<sup>74</sup>, and in the charophyte *Klebsormidium nitens*, after exposure to high light regimes<sup>75</sup>. Additionally, microalgae employ enzymes that aid in the accumulation of secondary metabolites, such as lipids and pigments. CAs are essential for maintaining acid-base homeostasis, regulating pH, facilitating plastid lipid formation, facilitating inorganic carbon uptake, and controlling photosynthetic membrane composition<sup>43,76,77</sup>. CAs function in coordination with the activity of the photosynthetic machinery and are affected by changes in the circadian light regime<sup>78</sup>. The question of whether there are synergistic effects between the mechanisms of cold-resistance, antioxidant defense and salinity tolerance in *Plocamionas psychrophila* CCMP2097 remains unresolved. Flavonoids, which can suppress the formation of ROS, are among the proteins that help to maintain the ROS balance<sup>79,80</sup> and were overexpressed. Furthermore, the overexpression of two DEGs coding CSS and CHI in the pelagophyte suggests that immediate antioxidant defense through secondary metabolites occurs upon perturbation.

Several essential genes with a role in stress tolerance were uncovered, including cazymes like GH18, a chitinase that acts in plant defense and induces resistance to biotic and abiotic stresses<sup>81,82</sup>. This response was previously seen in the brown alga, *Ascophyllum nodosum*, which survives in cold and frozen waters<sup>83</sup> and would maintain membrane integrity during stress. Algal polysaccharides have been exploited for their biostimulant and phytoprotective properties, as well as for the production of commercial fertilizers<sup>84</sup>. It appears that the pelagophyte can express a chitinase (GH18) upregulated at t2h in both lower salinities (Fig. 7 and Supplementary Fig. S10) to produce polysaccharides that might aid in the rapid adaptability of the cell membrane to changes in salinity. The cazyase AA2/katG is a catalase-peroxidase that is secreted into the extracellular environment<sup>21,85</sup>. This confers resistance against ROS<sup>21</sup> by facilitating the conversion of ROS to oxygen and water<sup>86</sup>. Two specific enzymes, katG (peroxidase) and ahpC (alkylhydroperoxyreductase), appear to be induced in response to oxidative stress<sup>45</sup>, and help the cell activate stress resistance to the new environment. The pelagophyte cell wall would be predicted to have multiple sensor proteins, including LRR, a leucine-rich repeat transmembrane protein that detects stress signals (Fig. 6). In the microalga *Neochloris oleoabundans*, an increase in leucine within the cell wall affected cell wall remodeling under varying growth conditions, highlighting the important role of LRR in stress responses<sup>87</sup>.

The cold-adapted genes in the pelagophyte are thought to have been acquired from other microorganisms, including other microalgae in the Arctic Ocean<sup>18</sup> and are useful in its current habitat. In contrast, the plethora of stress genes triggered by sudden changes in salinity appear to be ancient pathways found in plants and other eukaryotes, rather than being specific to the Arctic. Planktonic pelagophyte species are unicellular<sup>26</sup>, but several genera, including *Pelagomonas*, *Aureococcus* and *Aureoumbra*, can cause large-scale algal blooms, commonly known as “brown tides” in tropical and temperate waters<sup>27,28</sup>. While most brown tide studies concentrate on nutrient levels, a decrease in *Aureococcus* has been associated with slow estuarine flushing, where salinity increased in a barrier island lagoon<sup>88</sup>. Our work on an unrelated pelagophyte opens the possibility that salinity and other factors besides nutrients may influence such bloom-forming species, but more work needs to be done. The potential for pelagophyte blooms in the Arctic remains uncertain. Factors such as the time required for acclimatization and the ability of cells to react quickly to a new environment are measured at different time scales. We note that the cellular division in this unialgal culture grown under constant light is asynchronous and speculate that some portion of the cells could be more susceptible to stress during part of the cell cycle<sup>89</sup>. The genetic underpinning of mechanisms by which microalgae produce essential antioxidants, osmoprotectants, stress-response proteins and cold-adaptive proteins provides a window of understanding on how Arctic microbial eukaryotes regulate metabolism and ensure survival in a changing environment.

## Methods

### Pelagophyte isolation, culture, and collection

Originally, the Arctic pelagophyte CCMP2097 was collected in June 1998 from liquid pocket of water on the ice surface of Northern Baffin Bay, and isolated by serial dilution as described in ref. 25. The unialgal culture was deposited in at National Center for Marine Algae and Microbiota and cryopreserved. Fresh cultures were obtained several months prior to experiments and maintained at ca. 4 °C in L1 medium<sup>23,90</sup>.

To document the acute transcriptional response of pelagophyte CCMP2097 prior to homeostasis as reported by Freyria et al.<sup>25</sup>, we exposed the microalga to a sudden salinity change. We measured transcriptional gene expression at 0, 2, 6, 12 and 24h after transfer to lower salinity and compared it to transcriptomes following transfer to the new media at the same initial salinity (Supplementary Fig. S1a,b). For this, we initially grew the microalga at a higher salinity 45, which is within the range of that found in brine channels, then adjusted the salinity to either 22 or 16. Cultures of pelagophyte CCMP2097 acclimated to a salinity 45, were transferred to media adjusted to salinity 16 and 22. The cells were harvested at times t0h, t2h, t6h, t12h and t24h after the salinity adjustment. In parallel, control cultures were maintained at salinity 45 and harvested at the same times (Supplementary Fig. S1a,b).

The pelagophyte cultures were incubated in 2 L flasks using an Algem photobioreactor (Algenuity Ltd, UK). All cultures were grown in L1 medium with the addition of 1:10 of mixed antibiotics (25 mg L<sup>-1</sup> of Penicillin, 20 mg L<sup>-1</sup> of Kanamycin and 20 mg L<sup>-1</sup> Neomycin) to eliminate contaminant bacterial growth. The initial culture volume was 600 mL with an algal cell concentration of  $3 \times 10^7$  cells mL<sup>-1</sup>. Incubations conditions were kept constant. To mimic summer surface light conditions in the Arctic, cultures were grown at constant illumination of 100 μmol photons m<sup>-2</sup> s<sup>-1</sup> over 24 h. The culture flasks were constantly mixed at a rate of 40 rpm and temperature maintained at 5–6 °C, with biomass monitored as optical density (OD), measured every hour using Algem software v.1.4.5. Triplicate initial cultures were grown under the above conditions at a salinity of 45. The latent phase persisted four days and late exponential phase was reached on day 18. On day 18, 200 mL of initial salinity 45 cultures were transferred into a new autoclaved flasks with 400 mL of fresh medium (including 600 μL of fresh antibiotics) adjusted to the lower salinities (16 or 22), or at the same salinity of 45. Time 0 was taken to be at the moment of the transfer to new medium. The triplicate cultures for each salinity were subsequently sampled at 2 h, 6 h, 12 h and 24 h after transfer (Supplementary Fig. S1a,b).

### Nutrient concentrations and consumption and cell viability

To determine nutrient concentration in each culture, we used a syringe to collect 100 mL of culture. A volume of 30 mL was filtered through a glass fiber filter (Whitman GF/F) mounted in a 25 mm Swinnex filter holder. Nutrients were collected at time 0 h, 12 h, and 24 h. The filtrate was dispensed into two 15 mL Falcon tubes of each triplicate culture of all salinity condition. The Falcon tubes were vertically flash frozen into liquid nitrogen and stored at –80 °C until analysis. Nutrients (nitrate, nitrite and phosphate) were analyzed at Laval University, Québec using an Autoanalyser 3 with standard colorimetric methods<sup>91</sup>. To calculate nutrient consumption by cells, we followed the methodology previously described<sup>25</sup>, which involved subtracting the final concentration at the time of sampling from the initial concentration added at the start of the culture of the experiment (t0h).

To estimate cell viability, we used 2 mL from the 100 mL volume of culture collected from each triplicate at t0h, t12h and t24h to evaluate proportion of live and dead cells. Cells were stained with SYTOX Green Nucleic Acid Stain (Invitrogen, Thermofisher Scientific), which penetrates cells with compromised membranes that were considered dead. The non stained cells with natural chlorophyll fluorescence<sup>92</sup> were considered as live (Supplementary Fig. S12). Cells were counted on a; BD Accuri C6 Flow Cytometer (BD Biosciences<sup>25</sup>).

### Nucleic acid extraction, library preparation, and sequencing

At each of the five time points (t0h to t24h) for all salinity conditions, we used 30 mL from the 100 mL volume of cells collected to extract RNA from the cells. The particulate material (cells) from the 30 mL of culture were collected onto 0.22 µm pore size Sterivex filter units (Milipore). The Sterivex were then flash frozen by placing them into liquid nitrogen for 30 min and stored at  $-80^{\circ}\text{C}$  until RNA extraction. RNA was extracted from the Sterivex filter units as in Dasilva, et al.<sup>93</sup>, using the RNeasy mini kit (Qiagen). Quantification of RNA was verified using a Qubit fluorometer (Life Technologies, Invitrogen) with the RNA BR Assay Kit (Invitrogen) and the quality was checked with NanoDrop 8000 spectrophotometer (Thermo Scientific). After initial quality checks, the extracted RNA was sent to the Department of Energy (DOE) Joint Genome Institute (JGI) in Walnut Creek, California for RNA library preparation as in ref. 25. Samples were sequenced on an Illumina NovaSeq 6000 sequencer using NovaSeq XP V1 reagent kits, S4 flow cell, following the  $2 \times 150$  indexed run protocols at DOE JGI. An initial transcriptomic analysis was carried out at DOE JGI<sup>25</sup>.

### Transcriptomic analysis

From the 5 time points with 3 replicates and 3 conditions there were 45 initial samples, as some samples were sequenced twice at DOE JGI, to verify the runs, we obtained and analyzed 64 transcriptomes (Supplementary Table S5). The following analyses were conducted using Compute Canada (Digital Research Alliance) facilities. Clean reads from DOE JGI were trimmed using Trimmomatic v.0.36<sup>94</sup> with paired-end mode and minimum read length of 100 pb. All trimmed transcriptome reads were mapped separately onto the CCMP2097 reference genome available at JGI PhycoCosm Portal<sup>39</sup> using Spliced Transcripts Alignment to a Reference (STAR) v.2.7.8a<sup>95</sup> with default parameters. The mapped reads were counted using FeatureCounts<sup>96</sup> to evaluate the number of aligned read pairs to each gene between biological replicates. Overall, 19,402 genes models were mapped from the reference genome of pelagophyte CCMP2097 against all transcriptomes. The total number of clean reads generated for each sample ranged from 273,863 to 40,209,737 for salinity 16, from 262,048 to 35,487,445 for salinity 22, and from 476,541 to 28,902,528 for salinity 45. After the number of reads per gene were determined for each transcriptome, sequencing replicates were pooled.

Additionally, gene annotations were retrieved from the JGI Genome Portal with CCMP2097 as the reference genome<sup>39</sup>. Gene annotations included those from Gene Ontology (GO), Kyoto Encyclopedia of Genes and Genomes (KEGG), eukaryotic Ortholog Groups of proteins (KOG), signal peptide and Interproscan annotations. Carbohydrate active enzymes (CAZyme) were predicted using dbCAN, a web server for automated CAZyme annotation using hmmscan v.3.3.2 and based on the CAZy database<sup>97</sup>.

All further analyses were performed in the RStudio v.1.4.1106 environment. Counted mapped reads of all transcriptomes were normalized using DESeq2 package in R<sup>98</sup>, where counts are divided by sample-specific size factors determined by the median ratio of gene counts. This step was followed by differential gene expression analyses using DESeq2. Only genes with  $p$ -value adjusted  $\leq 0.05$  and with a threshold of absolute fold change (FC)  $\geq 2$  ( $\log_2 \text{FC} \geq 2$ ) were called and considered as significant differential expressed genes (DEGs) between conditions tested, which were time of sampling (t0h to t24h) between the salinity levels 16, 22 and 45 (control).

We performed Weighted Gene Co-expression Network Analysis (WGCNA) using WGCNA package<sup>99</sup> in R on significant DEGs between conditions to analyze salinity and time effects. To construct co-expression modules, we used default settings except with a soft thresholding power of 12 ( $n = 64$ ), minimum Module size was 30 genes, and a branch merge cut height of 0.25. Genes were clustered into 8 correlated modules. To identify the relationship between time of sampling and salinity conditions within all modules, the Pearson's correlation coefficient was calculated. Hub genes with the highest connectivity among each module were calculated using intramodular connectivity (K.in) and module correlation degree (MM) of

each gene. Hub genes may represent key genes with potentially important functions.

### Statistics and reproducibility

A two-way analysis of variance (ANOVA) without replication was conducted on the cell viability (triplicate,  $n = 3$ ), number of live and dead cells using Past4 v.4.11 software (Supplementary Table S2). Another two-way ANOVA, but with repeated measure was conducted to analyze the time effect between salinity change and control conditions on nutrient final concentration and consumption (two replicates for each triplicate,  $n = 6$ ) at t0h, t12h and t24h (Supplementary Table S3). Canonical Correspondence Analysis (CCA) was computed using *cca()* function from the *Vegan* package<sup>100</sup>, to discriminate different transcriptomes for each salinity condition according to the real salinity values measured at the time of sampling and the effect of time of sampling. A dendrogram was computed using *hclust()* function from the *Stats* package<sup>101</sup>. The complete linkage method was used to construct the dendrogram, which finds similar clusters among samples. Unweighted Pair Group Method with Arithmetic mean (UPGMA) tree was constructed in the QIIME environment<sup>102</sup> based on the Bray Curtis distance matrices of only significant DEGs from salinity 16 and 22 to show which samples were closer together depending on the time of sampling. The top 50 heatmap was computed on normalized and transformed read counts with *vst()* function in *DESeq2* and visualized with *heatmap()* function from *heatmap* package<sup>103</sup>. Circular heatmaps of selected DEGs were based on the normalized number of reads per gene and on values of  $\log_2 \text{FC}$  between comparison of sampling time among all salinity conditions, and were visualized using *circos.heatmap()* function in R from *circize* package<sup>104</sup>. To visualize the DEGs with differential gene expression relative to the log-fold change, we used scatter plots and volcano plots computed with *DESeq2* package. Networks of each module were visualized as previously described<sup>105</sup> and using Cytoscape v.3.9.1<sup>106</sup>. The node circle size is positively correlated with the number of genes that are partnered within interactions.

### Reporting summary

Further information on research design is available in the Nature Portfolio Reporting Summary linked to this article.

### Data availability

All transcriptome raw sequence data are in the DOE JGI Gold Portal under GOLD project ID Gp0452945 to Gp0452988 and under NCBI BioProject Accession PRJNA677358. CCMP 2097 annotated genome is available at the JGI Genome Portal under JGI Project ID 1020062 ([https://genome.jgi.doe.gov/portal/Pelago2097\\_1/Pelago2097\\_1.download.html](https://genome.jgi.doe.gov/portal/Pelago2097_1/Pelago2097_1.download.html)) and at PhycoCosm Portal ([https://phycocosm.jgi.doe.gov/Pelago2097\\_1](https://phycocosm.jgi.doe.gov/Pelago2097_1)).

### Code availability

This paper does not report original code. All code was adapted from the user manuals of the software packages. The coding script is available and data files at <https://osf.io/2deq7/>.

Received: 4 April 2024; Accepted: 21 August 2024;

Published online: 04 September 2024

### References

- Smith, M. M. et al. Quantifying false bottoms and under-ice meltwater layers beneath Arctic summer sea ice with fine-scale observations. *Elem. Sci. Anth.* **10**, 000116 (2022).
- Tremblay, J. É., Gratton, Y., Carmack, E. C., Payne, C. D. & Price, N. M. Impact of the large-scale Arctic circulation and the North Water Polynya on nutrient inventories in Baffin Bay. *J. Geophys. Res. Oceans* **107**, 26-21–26-14 (2002).
- Popova, E. et al. Control of primary production in the Arctic by nutrients and light: insights from a high resolution ocean general circulation model. *Biogeosciences* **7**, 3569–3591 (2010).



4. Tremblay, J.-É. et al. Global and regional drivers of nutrient supply, primary production and CO<sub>2</sub> drawdown in the changing Arctic Ocean. *Prog. Oceanogr.* **139**, 171–196 (2015).
5. Meier, W. N. et al. Arctic sea ice in transformation: A review of recent observed changes and impacts on biology and human activity. *Rev. Geophys.* **52**, 185–217 (2014).
6. Maslanik, J. et al. A younger, thinner Arctic ice cover: Increased potential for rapid, extensive sea-ice loss. *Geophys. Res. Lett.* **34**, <https://doi.org/10.1029/2007GL0320431> (2007).
7. Kwok, R. et al. Thinning and volume loss of the Arctic Ocean sea ice cover: 2003–2008. *J. Geophys. Res. Oceans* **114**, <https://doi.org/10.1029/2009JC0053121> (2009).
8. Feng, J., Zhang, Y., Cheng, Q. & Tsou, J. Y. Pan-Arctic melt pond fraction trend, variability, and contribution to sea ice changes. *Glob. Planet. Change* **217**, 103932 (2022).
9. Joli, N., Monier, A., Logares, R. & Lovejoy, C. Seasonal patterns in Arctic prasinophytes and inferred ecology of *Bathycoccus* unveiled in an Arctic winter metagenome. *ISME J.* **11**, 1372–1385 (2017).
10. Leu, E. et al. Arctic spring awakening—steering principles behind the phenology of vernal ice algal blooms. *Prog. Oceanogr.* **139**, 151–170 (2015).
11. Gêrikas Ribeiro, C. et al. Culturable diversity of Arctic phytoplankton during pack ice melting. *Elem. Sci. Anthr.* **8**, 6 (2020).
12. Kirst, G. Salinity tolerance of eukaryotic marine algae. *Annu. Rev. Plant Biol.* **41**, 21–53 (1990).
13. Maykut, G. A. The surface heat and mass balance. In *The Geophysics of Sea Ice* (ed Norbert Untersteiner), 395–463. [https://doi.org/10.1007/978-1-4899-5352-0\\_61](https://doi.org/10.1007/978-1-4899-5352-0_61) (Springer US, Springer Link, 1986).
14. Werner, I., Ikävalko, J., & Schünemann, H. Sea-ice algae in Arctic pack ice during late winter. *Polar Biol.* **30**, 1493–1504 (2007).
15. Cottier, F., Eicken, H. & Wadhams, P. Linkages between salinity and brine channel distribution in young sea ice. *J. Geophys. Res. Oceans* **104**, 15859–15871 (1999).
16. Zhulay, I., Iken, K., Renaud, P. E., Kosobokova, K. & Bluhm, B. A. Reduced efficiency of pelagic–benthic coupling in the Arctic deep sea during lower ice cover. *Sci. Rep.* **13**, 6739 (2023).
17. Chaffron, S. et al. Environmental vulnerability of the global ocean epipelagic plankton community interactome. *Sci. Adv.* **7**, eabg1921 (2021).
18. Dorrell, R. G. et al. Convergent evolution and horizontal gene transfer in Arctic Ocean microalgae. *Life Sci. Alliance* **6**, <https://doi.org/10.26508/lsa.2022018331> (2023).
19. Stephens, T. G. et al. Genomes of the dinoflagellate *Polarella glacialis* encode tandemly repeated single-exon genes with adaptive functions. *BMC Biol.* **18**, 56 (2020).
20. Kennedy, F., Martin, A., Bowman, J. P., Wilson, R. & McMinn, A. Dark metabolism: a molecular insight into how the Antarctic sea-ice diatom *Fragilariopsis cylindrus* survives long-term darkness. *N. Phytol.* **223**, 675–691 (2019).
21. Alharbi, A. et al. Role of peroxiredoxin of the AhpC/TSA family in antioxidant defense mechanisms of *Francisella tularensis*. *PLoS One* **14**, e0213699 (2019).
22. Koid, A. E. et al. Comparative transcriptome analysis of four prymnesiophyte algae. *PLoS One* **9**, e97801 (2014).
23. Terrado, R., Monier, A., Edgar, R. & Lovejoy, C. Diversity of nitrogen assimilation pathways among microbial photosynthetic eukaryotes. *J. Phycol.* **51**, 490–506 (2015).
24. Daugbjerg, N., Lara, C., Gai, F. F. & Lovejoy, C. *Plocamiomonas psychrophila* gen. et sp. nov. (Pelagophyceae, Heterokontophyta), an Arctic marine nanoflagellate characterized by microscopy, pigments and molecular phylogeny. *Eur. J. Phycol.*, 1–17, <https://doi.org/10.1080/09670262.2024.23539401> (2024).
25. Freyria, N. J. et al. Salinity tolerance mechanisms of an Arctic pelagophyte using comparative transcriptomic and gene expression analysis. *Commun. Biol.* **5**, 500 (2022).
26. Andersen, R. A., Saunders, G. W., Paskind, M. P. & Sexton, J. P. Ultrastructure and 18s rRNA gene sequence for *Pelagomonas calceolata* gen. et sp. nov. and the description of a new algal class, the Pelagophyceae Classis nov. 1. *J. Phycol.* **29**, 701–715 (1993).
27. Etheridge, S., Roesler, C. & Pitcher, G. C. Application of an Ocean Color Algal Taxa Detection Model to Red Tides in the Southern Benguela. <http://hdl.handle.net/1834/826> (Auquodocs, 2000).
28. Gobler, C. J. et al. Niche of harmful alga *Aureococcus anophagefferens* revealed through ecogenomics. *Proc. Natl Acad. Sci. USA* **108**, 4352–4357 (2011).
29. Wetherbee, R., Bringloe, T. T., van de Meene, A., Andersen, R. A. & Verbruggen, H. Structure and formation of the perforated theca defining the Pelagophyceae (Heterokonta), and three new genera that substantiate the diverse nature of the class. *J. Phycol.* **59**, 126–151 (2023).
30. Lovejoy, C., Massana, R. & Pedrós-Alió, C. Diversity and distribution of marine microbial eukaryotes in the Arctic Ocean and adjacent seas. *Appl. Environ. Microbiol.* **72**, 3085–3095 (2006).
31. Comeau, A. M., Li, W. K., Tremblay, J.-É., Carmack, E. C. & Lovejoy, C. Arctic Ocean microbial community structure before and after the 2007 record sea ice minimum. *PLoS One* **6**, e27492 (2011).
32. Lovejoy, C. Changing views of Arctic protists (marine microbial eukaryotes) in a changing Arctic. *Acta Protozool.* **53**, <https://doi.org/10.4467/16890027AP.14.009.14461> (2014).
33. Edgar, R. *Un premier aperçu de la diversité génétique de cinq microbes eucaryotique de l'océan arctique*, MSc. mémoire, Biologie, Université Laval (2015).
34. DeVries, A. Antifreeze peptides and glycopeptides in cold-water fishes. *Annu. Rev. Physiol.* **45**, 245–260 (1983).
35. Mazur, P. Freezing of living cells: mechanisms and implications. *Am. J. Physiol. Cell Physiol.* **247**, C125–C142 (1984).
36. Asulabh, K., Supriya, G. & Ramachandra, T. Effect of salinity concentrations on growth rate and lipid concentration in *Microcystis* sp., *Chlorococcum* sp. and *Chaetoceros* sp in *National Conference on Conservation and Management of Wetland Ecosystems*. <https://wgbis.ces.iisc.ac.in/energy/lake2012/index.htm> (Kottayam, Kerala, LAKE 2012).
37. Kan, G. et al. Acclimatory responses to high-salt stress in *Chlamydomonas* (Chlorophyta, Chlorophyceae) from Antarctica. *Acta Oceanol. Sin.* **31**, 116–124 (2012).
38. Briggs, M. S. & Gierasch, L. M. Molecular mechanisms of protein secretion: the role of the signal sequence. *Adv. Protein Chem.* **38**, 109–180 (1986).
39. Grigoriev, I. V. et al. PhycoCosm, a comparative algal genomics resource. *Nucl. Acids Res.* **49**, D1004–D1011 (2021).
40. Hutsul, J.-A. & Worobec, E. Molecular characterization of the *Serratia marcescens* OmpF porin, and analysis of *S. marcescens* OmpF and OmpC osmoregulation. *Microbiology* **143**, 2797–2806 (1997).
41. Maeda, T., Wurgler-Murphy, S. M. & Saito, H. A two-component system that regulates an osmosensing MAP kinase cascade in yeast. *Nature* **369**, 242–245 (1994).
42. Kappes, R. M., Kempf, B. & Bremer, E. Three transport systems for the osmoprotectant glycine betaine operate in *Bacillus subtilis*: characterization of OpuD. *J. Bacteriol.* **178**, 5071–5079 (1996).
43. Raven, J. A. Photosynthetic and non-photosynthetic roles of carbonic anhydrase in algae and cyanobacteria. *Phycologia* **34**, 93–101 (1995).
44. Glatz, J. C. & Luiken, J. F. Dynamic role of the transmembrane glycoprotein CD36 (SR-B2) in cellular fatty acid uptake and utilization. *J. Lipid Res.* **59**, 1084–1093 (2018).

45. Wehrly, T. D. et al. Intracellular biology and virulence determinants of *Francisella tularensis* revealed by transcriptional profiling inside macrophages. *Cell Microbiol.* **11**, 1128–1150 (2009).
46. Peschek, G. A., Obinger, C. & Renger, G. *Bioenergetic processes of cyanobacteria. From Evolutionary Singularity to Ecological Diversity.* (eds Peschek, G. A., Obinger, C., Renger, G.), 3–10, (Springer, 2011).
47. Bondarava, N., Un, S. & Krieger-Liszskay, A. Manganese binding to the 23 kDa extrinsic protein of Photosystem II. *Biochim. Biophys. Acta Bioenerg.* **1767**, 583–588 (2007).
48. Topçu, G. et al. A new flavone from antioxidant extracts of *Pistacia terebinthus*. *Food Chem.* **103**, 816–822 (2007).
49. Grabarek, Z. Structure of a trapped intermediate of calmodulin: calcium regulation of EF-hand proteins from a new perspective. *J. Mol. Biol.* **346**, 1351–1366 (2005).
50. Alotheid, H., Aldughaim, M. S. K., Alamri, S. S., Alrahimi, J. S. M. & Al-Jadani, S. H. Role of calcineurin biosignaling in cell secretion and the possible regulatory mechanisms. *Saudi J. Biol. Sci.* **28**, 116–124 (2021).
51. Gooch, J. L., Gorin, Y., Zhang, B.-X. & Abboud, H. E. Involvement of calcineurin in transforming growth factor- $\beta$ -mediated regulation of extracellular matrix accumulation. *J. Biol. Chem.* **279**, 15561–15570 (2004).
52. Lehner, R. & Quiroga, A. D. Fatty acid handling in mammalian cells. *Biochemistry of Lipids, Lipoproteins and Membranes (Seventh Edition)* (eds Ridgway, N. D. & McLeod, R. S.), 161–200 (Elsevier, 2021).
53. Heidrich, J., Thurotte, A. & Schneider, D. Specific interaction of IM30/Vipp1 with cyanobacterial and chloroplast membranes results in membrane remodeling and eventually in membrane fusion. *Biochim. Biophys. Acta Biomembr.* **1859**, 537–549 (2017).
54. Bar Dolev, M., Braslavsky, I. & Davies, P. L. Ice-binding proteins and their function. *Annu. Rev. Biochem.* **85**, 515–542 (2016).
55. Sarker, U., Islam, M. T. & Oba, S. Salinity stress accelerates nutrients, dietary fiber, minerals, phytochemicals and antioxidant activity in *Amaranthus tricolor* leaves. *PLoS One* **13**, e0206388 (2018).
56. Tolay, I. The impact of different Zinc (Zn) levels on growth and nutrient uptake of *Basil (Ocimum basilicum L.)* grown under salinity stress. *PLoS One* **16**, e0246493 (2021).
57. Tremblay, J.-É. & Gagnon, J. The effects of irradiance and nutrient supply on the productivity of Arctic waters: a perspective on climate change. *Influence of Climate Change on the Changing Arctic and Sub-Arctic Conditions* (ed Nihoul, J. C. J. & Kostianoy, A. G.), 73–93 (Springer, 2009).
58. Herdean, A. et al. A voltage-dependent chloride channel fine-tunes photosynthesis in plants. *Nat. Commun.* **7**, 11654 (2016).
59. Ambruster, U. et al. Ion antiport accelerates photosynthetic acclimation in fluctuating light environments. *Nat. Commun.* **5**, 5439 (2014).
60. Zuluaga, M., Gueguen, V., Pavon-Djavid, G. & Letourneur, D. Carotenoids from microalgae to block oxidative stress. *Bioimpacts* **7**, 1–3 (2017).
61. Di Pietro, N., Di Tomo, P. & Pandolfi, A. Carotenoids in cardiovascular disease prevention. *JSM Atheroscler.* **1**, 1002 (2016).
62. Krivoruchko, A., Zhang, Y., Siewers, V., Chen, Y. & Nielsen, J. Microbial acetyl-CoA metabolism and metabolic engineering. *Metab. Eng.* **28**, 28–42 (2015).
63. Small, G. D., Min, B. & Lefebvre, P. A. Characterization of a *Chlamydomonas reinhardtii* gene encoding a protein of the DNA photolyase/blue light photoreceptor family. *Plant Mol. Biol.* **28**, 443–454 (1995).
64. Kavakli, I. H., Ozturk, N. & Gul, S. DNA repair by photolyases. *Advances in Protein Chemistry and Structural Biology* (ed. R. Donev) **115**, 1–19 (Academic Press, 2019).
65. Mutsuda, M., Michel, K.-P., Zhang, X., Montgomery, B. L. & Golden, S. S. Biochemical properties of CikA, an unusual phytochrome-like histidine protein kinase that resets the circadian clock in *Synechococcus elongatus* PCC 7942\*. *J. Biol. Chem.* **278**, 19102–19110 (2003).
66. Somers, D. E., Devlin, P. F. & Kay, S. A. Phytochromes and cryptochromes in the entrainment of the *Arabidopsis* circadian clock. *Science* **282**, 1488–1490 (1998).
67. Coesel, S. N. et al. Diel transcriptional oscillations of light-sensitive regulatory elements in open-ocean eukaryotic plankton communities. *Proc. Natl Acad. Sci. USA* **118**, e2011038118 (2021).
68. Xing, W. & Rajashekar, C. Glycine betaine involvement in freezing tolerance and water stress in *Arabidopsis thaliana*. *Environ. Exp. Bot.* **46**, 21–28 (2001).
69. Diamant, S., Eliahu, N., Rosenthal, D. & Goloubinoff, P. Chemical chaperones regulate molecular chaperones in vitro and in cells under combined salt and heat stresses. *J. Biol. Chem.* **276**, 39586–39591 (2001).
70. Möker, N., Reihlen, P., Krämer, R. & Morbach, S. Osmosensing properties of the histidine protein kinase MtrB from *Corynebacterium glutamicum*. *J. Biol. Chem.* **282**, 27666–27677 (2007).
71. Rönsch, H., Krämer, R. & Morbach, S. Impact of osmotic stress on volume regulation, cytoplasmic solute composition and lysine production in *Corynebacterium glutamicum* MH20-22B. *J. Biotechnol.* **104**, 87–97 (2003).
72. Hancock, J., Desikan, R. & Neill, S. Role of reactive oxygen species in cell signalling pathways. *Biochem. Soc. Trans.* **29**, 345–349 (2001).
73. Fujiwara, T., Hirooka, S., Ohbayashi, R., Onuma, R. & Miyagishima, S.-Y. Relationship between cell cycle and diel transcriptomic changes in metabolism in a unicellular red alga. *Plant Physiol.* **183**, 1484–1501 (2020).
74. Lv, H. et al. Comparative transcriptome analysis of short-term responses to salt and glycerol hyperosmotic stress in the green alga *Dunaliella salina*. *Algal Res.* **53**, 102147 (2021).
75. Serrano-Pérez, E. et al. Transcriptomic and metabolomic response to high light in the charophyte alga *Klebsormidium nitens*. *Front. Plant Sci.* **13**, 855243 (2022).
76. Hoang, C. V. & Chapman, K. D. Biochemical and molecular inhibition of plastidial carbonic anhydrase reduces the incorporation of acetate into lipids in cotton embryos and tobacco cell suspensions and leaves. *Plant Physiol.* **128**, 1417–1427 (2002).
77. Sinetova, M. A., Kupriyanova, E. V., Markelova, A. G., Allakhverdiev, S. I. & Pronina, N. A. Identification and functional role of the carbonic anhydrase Cah3 in thylakoid membranes of pyrenoid of *Chlamydomonas reinhardtii*. *Biochim. Biophys. Acta Bioenerg.* **1817**, 1248–1255 (2012).
78. Jensen, E. L., Maberly, S. C. & Gontero, B. Insights on the functions and ecophysiological relevance of the diverse carbonic anhydrases in microalgae. *Int. J. Mol. Sci.* **21**, 2922 (2020).
79. Corradini, E. et al. Flavonoids: chemical properties and analytical methodologies of identification and quantitation in foods and plants. *Nat. Prod. Res.* **25**, 469–495 (2011).
80. Blas-Valdivia, V. et al. Microalgae of the Chlorophyceae class: potential nutraceuticals reducing oxidative stress intensity and cellular damage. *Oxidative Stress and Diseases* (ed Lushchak, V. I. and Gospodaryov, D. V.), **626** (IntechOpen, 2012).
81. Stadnik, M. J. & Freitas, M. B. D. Algal polysaccharides as source of plant resistance inducers. *Trop. Plant Pathol.* **39**, 111–118 (2014).
82. Rachidi, F., Benhima, R., Kasmi, Y., Sbabou, L. & Arroussi, H. E. Evaluation of microalgae polysaccharides as biostimulants of tomato plant defense using metabolomics and biochemical approaches. *Sci. Rep.* **11**, 930 (2021).
83. Rayirath, P. et al. Lipophilic components of the brown seaweed, *Ascophyllum nodosum*, enhance freezing tolerance in *Arabidopsis thaliana*. *Planta* **230**, 135–147 (2009).

84. Khan, W. et al. Seaweed extracts as biostimulants of plant growth and development. *J. Plant Growth Regul.* **28**, 386–399 (2009).
85. Ma, Z. et al. EmrA 1 membrane fusion protein of *Francisella tularensis* LVS is required for resistance to oxidative stress, intramacrophage survival and virulence in mice. *Mol. Microbiol.* **91**, 976–995 (2014).
86. Levasseur, A., Drula, E., Lombard, V., Coutinho, P. M. & Henrissat, B. Expansion of the enzymatic repertoire of the CAZy database to integrate auxiliary redox enzymes. *Biotechnol. Biofuels* **6**, 1–14 (2013).
87. Rashidi, B., Dechesne, A., Rydahl, M. G., Jørgensen, B. & Trindade, L. M. *Neochloris oleoabundans* cell walls have an altered composition when cultivated under different growing conditions. *Algal Res.* **40**, 101482 (2019).
88. Gobler, C. J. et al. Accidental ecosystem restoration? Assessing the estuary-wide impacts of a new ocean inlet created by Hurricane Sandy. *Estuar. Coast Shelf Sci.* **221**, 132–146 (2019).
89. Miyagishima, S.-Y. et al. Day/night separation of oxygenic energy metabolism and nuclear DNA replication in the unicellular red alga *Cyanidioschyzon merolae*. *MBio* **10**, 10–1128 (2019).
90. Guillard, R. R. Division rates. *Handbook of Phycological Methods, Culture Methods and Growth Measurements* (ed Stein, J. R.), 289–311 (Cambridge University Press, 1973).
91. Grasshoff, K., Ehrhardt, M. & Kremling, K. *Methods of Seawater Analysis. 3rd.* (Weinheim: Verlag Chemie GmbH, 1999).
92. Dashkova, V., Malashenkov, D., Poulton, N., Vorobjev, I. & Barteneva, N. S. Imaging flow cytometry for phytoplankton analysis. *Methods* **112**, 188–200 (2017).
93. Dasilva, C. R., Li, W. K. & Lovejoy, C. Phylogenetic diversity of eukaryotic marine microbial plankton on the Scotian Shelf Northwestern Atlantic Ocean. *J. Plankton Res.* **36**, 344–363 (2014).
94. Bolger, A. M., Lohse, M. & Usadel, B. Trimmomatic: a flexible trimmer for Illumina sequence data. *Bioinform* **30**, 2114–2120 (2014).
95. Dobin, A. & Gingeras, T. R. Mapping RNA-seq reads with STAR. *Curr. Protoc. Bioinform.* **51**, 11.14.11–11.14.19 (2015).
96. Liao, Y., Smyth, G. K. & Shi, W. Featurecounts: an efficient general purpose program for assigning sequence reads to genomic features. *Bioinform* **30**, 923–930 (2014).
97. Cantarel, B. L. et al. The Carbohydrate-Active EnZymes database (CAZy): an expert resource for glycogenomics. *Nucl. Acids Res.* **37**, D233–D238 (2009).
98. Love, M. I., Huber, W. & Anders, S. Moderated estimation of fold change and dispersion for RNA-seq data with DESeq2. *Genome Biol.* **15**, 1–21 (2014).
99. Langfelder, P. & Horvath, S. WGCNA: an R package for weighted correlation network analysis. *BMC Bioinform.* **9**, 559 (2008).
100. Dixon, P. & VEGAN a package of R functions for community ecology. *J. Veg. Sci.* **14**, 927–930 (2003).
101. R. Core Team. *The R Stats Package* <https://CRAN.R-project.org/package=STAT> (2018).
102. Caporaso, J. G. et al. QIIME allows analysis of high-throughput community sequencing data. *Nat. Methods* **7**, 335–336 (2010).
103. Kolde, R. Package “pheatmap”. *R package* **1**, 790 <https://CRAN.R-project.org/package=pheatmap> (2015).
104. Gu, Z., Gu, L., Eils, R., Schlesner, M. & Brors, B. Circlize implements and enhances circular visualization in R. *Bioinformatics* **30**, 2811–2812 (2014).
105. de Oliveira, T. C. et al. Unraveling the transcriptional features and gene expression networks of pathogenic and saprotrophic *Ophiostoma* species during the infection of *Ulmus americana*. *Microbiol. Spectr.* **12**, e03694–03623 (2024).
106. Shannon, P. et al. Cytoscape: a software environment for integrated models of biomolecular interaction networks. *Genome Res.* **13**, 2498–2504 (2003).

## Acknowledgements

We thank Marianne Potvin for data management, laboratory, and analytical support. We thank Eric Pelletier and Arnaud Meng from Genoscope, CEA, Evry, France for bioinformatics advice. We also are grateful to G. Deslongchamps from the Jean-Éric Tremblay Nutrient Laboratory for analyzing nutrient data with support from the project NTRAIN within ArcticNet, a Network of Centers of Excellence of Canada. We acknowledge the extensive team at DOE JGI for sequencing and protocols. The study was funded by Natural Sciences and Engineering Research Council of Canada (NSERC) Discovery program grants to C.L. Support from the Canada First Research Excellence Fund to Sentinelle Nord is acknowledged. Additional support was by way of the Fonds de recherche du Québec - Nature et Technologies (FRQNT) for Québec Océan and an FRQNT Team grant to C.L. The analyses were conducted using Digital Research Alliance of Canada-Compute Canada facilities. The work (10.46936/10.25585/60001017) conducted by the U.S. Department of Energy Joint Genome Institute (<https://ror.org/04xm1d337>), a DOE Office of Science User Facility, is supported by the Office of Science of the U.S. Department of Energy under Contract No. DE-AC02-05CH11231.

## Author contributions

Conceptualization, C.L. and N.J.F.; Methodology, N.J.F., M.C. and J.J.; Investigation, N.J.F., T.C.O. and A.L.; Writing – Original Draft, N.J.F. and C.L.; Visualization, N.J.F. and T.C.O.; Writing – Review & Editing, N.J.F., T.C.O., C.L. and I.V.G.; Funding Acquisition, C.L.; Resources, C.L., K.W.B., I.V.G., and A.K. Supervision, C.L.

## Competing interests

The authors declare no competing interests.

## Additional information

**Supplementary information** The online version contains supplementary material available at <https://doi.org/10.1038/s42003-024-06765-7>.

**Correspondence** and requests for materials should be addressed to Nastasia J. Freyria or Connie Lovejoy.

**Peer review information** *Communications Biology* thanks Thomas Mock and the other, anonymous, reviewer(s) for their contribution to the peer review of this work. Primary Handling Editors: Dr Linn Hoffmann and Dr Ophelia Bu. A peer review file is available.

**Reprints and permissions information** is available at <http://www.nature.com/reprints>

**Publisher's note** Springer Nature remains neutral with regard to jurisdictional claims in published maps and institutional affiliations.

**Open Access** This article is licensed under a Creative Commons Attribution-NonCommercial-NoDerivatives 4.0 International License, which permits any non-commercial use, sharing, distribution and reproduction in any medium or format, as long as you give appropriate credit to the original author(s) and the source, provide a link to the Creative Commons licence, and indicate if you modified the licensed material. You do not have permission under this licence to share adapted material derived from this article or parts of it. The images or other third party material in this article are included in the article's Creative Commons licence, unless indicated otherwise in a credit line to the material. If material is not included in the article's Creative Commons licence and your intended use is not permitted by statutory regulation or exceeds the permitted use, you will need to obtain permission directly from the copyright holder. To view a copy of this licence, visit <http://creativecommons.org/licenses/by-nc-nd/4.0/>.

© The Author(s) 2024